Experimental and Numerical Investigation on Thermal Management of an Outdoor Battery Cabinet

X.Z. Meng[1], Z. Lu[1], L.W. Jin[1*], L.Y. Zhang[1], W.Y. Hu[2], L.C. Wei[3], J. C. Chai[4]
[1]Department of Building Environment and Energy Engineering, Xi'an Jiaotong University, Shaanxi, 710049, China.
[2]Chinese Association of Refrigeration, Beijing, 100142, China.
[3]Shenzhen Envicool Technology Co. Ltd., Shenzhen, 518129, China.
[4]Department of Engineering and Technology, School of Computing and Engineering, University of Huddersfield, HD1 3DH, U.K.
[*]Corresponding author: lwjin@mail.xjtu.edu.cn

Abstract

Many forms of electronic equipment such as battery packs and telecom equipment must be stored in harsh outdoor environment. It is essential that these facilities be protected from a wide range of ambient temperatures and solar radiation. Temperature extremes greatly reduce lead-acid based battery performance and shorten battery life. Therefore, it is important to maintain the cabinet temperature within the optimal values between 20^{o}C and 30^{o}C to ensure battery stability and to extend battery lifespan. To this end, cabinet enclosures with proper thermal management have been developed to house such electronic equipment in a highly weather tight manner, especially for battery cabinet.

In this paper, the flow field and temperature distribution inside an outdoor cabinet are studied experimentally and numerically. The battery cabinets house 24 batteries in two configurations namely, two-layer configuration and six-layer configuration respectively. The cabinet walls are maintained at a constant temperature by a refrigeration system. The cabinet's ability to protect the batteries from an ambient temperature as high as 50^{o}C is studied. An experimental facility is developed to measure the battery surface temperatures and to validate the numerical simulations. The differences between the experimental and computational fluid dynamic (CFD) results are within 5%.

Keywords: battery cabinet; temperature uniformity; natural convection; air circulation; radiation

Nomenclature

d_{ci}	inner diameter of capillary (mm)	S_ϕ	source term
d_{co}	outer diameter of steel tube (mm)	T_{amb}	ambient environments (^oC)
d_{eo}	outer diameter of aluminum tube (mm)	W	width(mm)
d_w	the diameter of steel wire (mm)	X, Y, Z	directions
g	acceleration due to gravity (9.8 m/s^2)	*Greek symbols*	
H	height(mm)	ρ	density of fluid (kg/m^3)
L	length (mm)	ϕ	general variables
l_{tc}	tube space of aluminum tube (mm)	Γ_ϕ	generalized diffusion coefficient

1. Introduction

Outdoor cabinets are used to house many forms of electronic equipment, from battery packs to telecom equipment. The outdoor cabinet serves two purposes: (1) to provide storage space which is not available inside existing building and (2) to protect the electronic equipment from adverse outdoor environmental conditions and solar radiation. As the electronic equipment usually generates considerable amounts of heat during operation, these outdoor cabinets must come with proper thermal management system to ensure optimal operations. Over the last two decades, several thermal management systems have been used to keep the battery packs at an optimum temperature with small temperature variations. The dynamic behavior of the batteries during thermal runaway is reported and thermal runaway may be caused by a perturbation of the steady state conditions [1]. A novel system based on peltier-effect heat pump for thermal management of electric/hybrid vehicles has been described [2]. A new battery thermal management method using a reciprocating air flow for cylindrical Li-ion cells shows that the reciprocating flow can reduce the cell temperature difference of the battery system [3]. The advantages of liquid cooling/heating and phase change materials (PCMs) over air cooled have been reported [4-8]. The effectiveness of PCMs for Li-ion batteries which exhibit a net cooling effect during charge and highly exothermic during discharge has also been reported [9]. Recently, the thermal conductivity of PCM has also been significantly improved by impregnating an expanded graphite matrix with the PCM [10]. Four different methods of heat dissipation, natural convection cooling, presence of aluminum foam heat transfer matrix, use of PCM and combination of

aluminum foam and PCM have been investigated [11]. It is found that not only the use of aluminum foam with PCM can lower temperature rise than the use of either PCM or aluminum foam, but also keep the temperature uniform within the battery module.

From the above literature review, it is clear that major efforts have been carried out on thermal management of individual battery to keep its temperature uniform. Not much work has been reported on the thermal management of battery cabinets of which house a specific number of batteries to be protected from harsh outdoor environment. In the actual application of outdoor battery cabinet exposed to harsh environment, the protection levels of these cabinets should meet IP65 to make sure that the batteries operate safely and effectively. A key performance indicator of a battery cabinet is in its ability to maintain the temperatures of the batteries within a desirable range. The desired operating temperature range is different for various battery types. For a lead-acid battery, the optimum temperature is between 20^{o}C and 30^{o}C. Without proper thermal management, battery packs can easily reach 80^{o}Cduring periods of sustained discharge or rapid charging [12]. As battery life is cut by half for every 10^{o}C increase in temperature, properly thermal managed battery cabinets which can maintain the battery temperatures within the optimal values between 20^{o}C and 30^{o}C are critical to the long term operations of the batteries. In addition to maintaining between the optimal temperatures, battery packs also need to be operating at uniform temperatures. Temperature non-uniformities result in different charge/discharge behaviors, which causes electrically unbalanced modules and the reduction of battery packs' performance [13]. Therefore, it is important to maintain the battery cabinet optimum temperature and temperature uniformity for ensuring battery stability and extending battery lifespan through proper thermal management system.

Outdoor temperature with large fluctuations and the heat generated by the battery itself make the air cooling insufficient to maintain the battery operating temperature. Furthermore, an outdoor battery cabinet has to fulfill certain IP (Ingress Protection) standard to avoid rainwater/dust entering the cabinet. In this research, therefore, a commercial refrigeration system is applied to maintain the desired temperature on the cabinet wall. Then, the study focuses on the investigation of the performance of a passive air cooling system utilizing natural convection without moving parts inside the battery cabinet is analyzed. A DC powered mini air conditioning system was installed on the battery cabinet frame to maintain the cabinet internal wall temperature at a specified value of 17^{o}C in this study. The study

focuses on the investigation of the flow fields and temperature distributions inside battery cabinets where 24 batteries were placed by two configurations. The surface temperatures of different batteries were measured experimentally. Using experimental data as the boundary conditions, comprehensive flow motion and heat transfer phenomena inside the outdoor battery cabinet were numerically investigated and analyzed in this article.

2. Experimental Measurements

2.1. Experimental Facility

Figure 1(a) shows the schematic of a static outdoor battery cabinet without ventilation placed inside a temperature-controlled chamber. The chamber simulates external environment encountered by the battery cabinet. The chamber air was heated by two electric heaters producing a total heat load of 1000W. An intelligent temperature controller (SIEMENS, RLU222) was used to modulate the chamber temperature. Two fans hanging on the side walls of the chamber were used to circulate air flow to keep the chamber temperature uniform. It is interesting to study the transient evolution of the temperature inside the battery cabinet. However, the objectives of the article is to examine the capabilities of the design to handle extreme conditions. The ambient temperatures of 30^{o}C and 50^{o}C represent two typical weather faced by outdoor battery cabinet in summer, i.e., mild and extreme conditions, respectively. As a result, the steady-state solutions of the system subjected to 30^{o}C and 50^{o}C were examined. As the systems can handle these typical weather, it will have no trouble dealing with the less severe situations where the daily temperatures cycle between daily high and low.

The external dimensions of the battery cabinet are 900 mm × 925 mm × 1830 mm and the internal dimensions of the same are 800 mm × 840 mm × 1730 mm. The internal dimensions are shown in Fig. 1(b). The 50 mm thickness cabinet wall is composed of a 46 mm polyurethane insulating layer sandwiched between two 2 mm metal sheets. An R134a vapor compression refrigeration system was used to maintain the cabinet walls at a specified temperature. The refrigeration system consisted of a compressor, an evaporator (parallel flow type, outer diameter d_{eo} = 6 mm and tube space l_{tc} = 50 mm), a condenser (tube-fin, outer diameter of steel tube d_{co} = 6 mm and diameter of steel wire d_{w} = 1.5 mm) and a capillary tube (inner diameter d_{ci} = 0.66 mm and length l_{c} = 0.5 m). The nominal cooling capacity of the mini compressor (HITACHI, BSA357CV-R1AN) is 365W. The evaporator was installed inside the two vertical side walls and the vertical back wall of the battery cabinet to maintain the temperature

of the three internal surfaces of the battery cabinet. For ease of discussion, these three walls are referred to as the cold walls in the remainder of this article. The condenser was placed outside the vertical wall of the environment chamber. It is important to note that the refrigeration system is a commercialized product which was used to maintain the cold wall temperature. The objective of this research is to study the possibility and method of protecting the batteries when the specified temperature is maintained by the nature convection inside the cabinet.

In this study, the cabinet was designed to house 24 valve-regulated lead-acid batteries. Each battery measures 200 mm × 180 mm × 340 mm and dissipates 69 W heat. The 24 batteries can be placed in two, three, four and six layers arrangements within the cabinet. Our analyses showed that the two and six layers configurations produce the largest temperature non-uniformities in the batteries. The temperature non-uniformities in the three and four layers configurations are much smaller and the absolute temperatures are within the desirable limits. As a result, two batteries storage arrangements of two-layer [Fig. 2(a)] and six-layer [Fig. 2(b)] were investigated to provide specific guidelines for the battery cabinet configured with 24 batteries. The two-layer configuration placed 12 batteries on each layer, while the six-layer arrangement was configured with 4 batteries for each layer.

2.2. Measurement and Data Reduction

The system was equipped with calibrated T type thermocouples with a precision of ±0.5^{o}C to measure the ambient temperature of the chamber, the temperatures of the battery surfaces and the internal surface temperatures of the cold walls (left, right and back walls). For the two-layer arrangement, the surface temperatures of the batteries were measured at two heights of 0.33 m and 1.1 m respectively. For the six-layer configuration, the batteries surface temperatures were measured at six heights corresponding to 0.2 m, 0.5 m, 0.8 m, 1.0 m, 1.3 m and 1.5 m, respectively. Fig. 3 shows the locations of the thermocouples for both configurations. The cold walls internal surface temperatures were measured at 0.3 m, 0.9 m and 1.5 m as shown in Fig. 4. Thermocouples were placed on the vertical central lines of these three walls. All data were collected by a data acquisition system composed of Agilent (34972A) and a computer. The temperatures were recorded with a time interval of 20 seconds.

Generally, experimental errors are classified into the random error and the systematic error. The time-averaged method was used to minimize the random error and careful experimentation and

precision apparatus were employed to eliminate the systematic error. The internal cold walls temperature was maintained at 17°C with a precision of ±1°C. When the battery surface temperature fluctuation was less than ±0.5°C, it is considered that the thermal steady state has been reached.

3. Numerical Simulations

3.1. Airflow Modeling

In this article, the air flow and temperature distributions in the battery cabinet were numerically simulated using Fluent 6.3.26. For the coupled convection and radiation in a closed cavity, the discrete ordinates model are used widely to solve the problems [14, 15]. Therefore, the discrete ordinates method was adopted to solve the radiative transfer equation. The flow was assumed to be steady, three-dimensional, incompressible and turbulent. The Boussinesq approximation was used to model the buoyancy effects. Turbulence was resolved using the standard k-ε turbulence model.

The general conservation equation is defined as

$$\frac{\partial(\rho\phi)}{\partial t} + div(\rho U\phi) = div(\Gamma_\phi grad\phi) + S_\phi \tag{1}$$

where ρ is the density of the fluid, $U = (u, v, w)$ is the velocity vector, Γ_ϕ is the generalized diffusion coefficient and S_ϕ is the source term. All the variables (velocities, temperature, turbulent energy and dissipation energy) to be solved were denoted by ϕ. With properly prescribed Γ_ϕ, S_ϕ and ϕ, Eq. (1) can be taken as the continuity, momentum, energy or other scalar equations respectively.

3.2. Boundary Conditions

The thermal boundary conditions were set according to the experimental measurements. Table 1 shows all thermal boundary conditions used for the two ambient temperatures of 30°C and 50°C. The wall heat fluxes were obtained by heat flux meter (Gardon XE-239). Two heat flux meters were installed respectively on top and bottom horizontal walls to measure these heat fluxes. For front vertical wall, however, three heat flux meters from bottom to top were used to measure the wall heat flux. The front vertical wall heat flux set in the simulation is an average value of the above measured three heat fluxes. For battery packs, heat flux meters were used to measure battery surfaces heat fluxes and found that heat fluxes on battery surfaces are rather uniform. For the sake of simplicity in this simulation, all battery surfaces were assumed to have uniform heat fluxes. All wall boundaries were modelled using the no-slip boundary condition and assumed to be black in the radiative heat transfer calculations.

3.3. Numerical Scheme

The grid was generated using the Gambit 2.4.6 pre-processor and the discretization of the computational domain was achieved using an unstructured mesh. The minimum distance between the batteries is 10 mm in battery cabinet. Therefore, finer meshes were used between the batteries in order to gain a better insight into flow field and temperature distributions around the batteries. The grid independency analysis was carried out to ensure that the numerical results are not influenced by the cell numbers. For the two-layer configuration, three grid systems, 180 × 82 × 84 (coarse), 180 × 82 × 168 (regular) and 180 × 82 × 252 (fine) control volumes were used. The horizontal temperature differences for the distance of 0.33 m from the bottom wall between the coarse mesh and the regular mesh and between the regular mesh and the fine mesh were 5% and 0.5% respectively. Three sets of computational meshes, 180 × 82 × 90 (coarse), 180 × 164 × 90 (regular) and 180 × 246 × 90 (fine) were used for the six-layer configuration. The vertical temperature differences on the symmetry plane between the coarse mesh and the regular mesh, and between the regular mesh and the fine mesh were 3% and 0.5% respectively. Therefore, the regular meshes are summarized in Table 2. The solution method was based on the following main hypothesis: Green-Gauss Node Based was adopted to discretize diffusion terms and the second-order upwind scheme for convective terms was used to reduce the numerical diffusion. The coupled velocity-pressure terms were resolved using the SIMPLE algorithm.

4. Results and Discussion

4.1. Experimental Data

Two-Layer Arrangement: Figures 5(a) and 5(b) show the temperature profiles of two vertical heights at 0.33 m and 1.1 m for chamber temperatures of 30^{o}C and 50^{o}C respectively. From Fig. 5(a), it can be seen that the surface temperatures of the battery packs are uneven at those two heights. As hot air rises, the surface temperatures of the batteries increase with height. As expected, the battery surface temperatures near the cold wall are lower than the temperatures around the center of battery cabinet. When the chamber temperature is raised to 50^{o}C as shown in Fig. 5(b), the battery surface temperatures for given heights are about 0.7^{o}C higher than those of the chamber temperature maintained at 30^{o}C. The temperature variations under the two ambient temperatures are similar. Meanwhile, the vertical temperature gradients between heights of 0.33 m and 1.1 m are found to be

1.95-2.60^{o}C/m. This indicates that the overall temperature profile is rather uneven in the battery cabinet with two-layer configuration for 24 batteries.

Six-Layer Arrangement: The vertical temperature profiles on the center plane of 0.42 m for the two ambient temperatures of 30^{o}C and 50^{o}C are shown in Figs. 6(a) and 6(b) respectively. For ambient temperature set at 30^{o}C, the battery surface temperatures increase with the height and the surface temperatures of batteries located at the center of cabinet are slightly higher than those near the cold walls at a same height. When ambient temperature rises to 50^{o}C, it is observed that the battery surface temperatures increase by an average of 1.0^{o}C in comparison with the ambient temperature set to 30^{o}C, the trends are similar.

Remarks: Based on the above discussion, it is found that the surface temperatures of battery packs increase with the height due to the effect of buoyancy effect for both configurations. The two-layer configuration with 12 batteries arranged tightly in each layer leads to higher surface temperatures of the battery packs than the six-layer arrangement. The temperature distribution of the six-layer configuration is relatively uniform at a given height. For the situations tested, the battery cabinet is able to keep the surface temperatures of the batteries between 20^{o}C and 30^{o}C.

4.2. Validation of Numerical Model

The numerical model is first validated using the measured data before further discussion on the detailed flow and temperature fields. Fig. 7 shows the comparison between experimental measurement and numerical solution subjected to ambient temperature of 30^{o}C. It is found that the numerical results are in good agreement with experimental data for both configurations. The differences between the numerical predictions and the experimental measurements are within 5%. Although not shown, agreements at other locations and ambient temperature of 50^{o}C are within the same deviation.

4.3. Temperature fields

Figures 8(a) and 8(b) show the temperature fields at the center plane of 0.42 m in the battery cabinets for the two ambient temperatures and the two-layer configuration. As expected, it is seen that the temperature fields for both cases on the symmetry planes of Y = 0.42 m are symmetrical between left and right vertical cold walls which are kept at 17^{o}C. Due to the close proximity of the twelve batteries in each of the two layers, most air flows through the side openings thus by-passing the small gaps between the batteries. As a result, the temperature rises are concentrated near the two layers of

batteries. Due to the moving air, the temperature is quite uniform in the open area away from the batteries. The temperatures near the front wall are higher than those near the back cold walls. The temperatures near the front walls are still lower than the hot air temperatures between the batteries. In addition, when ambient temperature set at 30^{o}C, it is observed from FLUENT Flux Reports that the radiation heat transfer accounts for about 47.8% of the total heat transfer and the natural convection heat transfer takes up about 52.2%. The analysis indicates that the radiation is of great importance in this coupling simulation.

For the six-layer configuration, however, the temperature increases gradually with height. This is due to less densely packed batteries at each of the six layers with smaller heat concentration and also the larger gaps for air to flow in between batteries. Meanwhile, significant thermal stratification is observed within the cold zone at the bottom of the battery cabinet and the warm zone at the top which is particularly noticeable for the ambient temperature kept at 50^{o}C.

Comparing the data shown in Figs. 8(c) and 9(c), the temperature fields on the symmetry planes of X = 0.40 m are not symmetrical between front vertical wall and back vertical cold wall. This is due to different boundary conditions for two vertical walls. The air temperature is hotter near the front wall than that near the rear wall because hot air rises along the front wall and sinks along the cold rear wall. When the ambient temperature is set at 50^{o}C, the temperature near the top of the front wall is about 3^{o}C higher than the temperature near the top of the rear wall. The large temperature difference enhances air circulation from the front vertical wall to the back vertical cold wall as shown in Fig. 8(d), which can be confirmed by the air velocity field discussed later in this article.

The properties of lead-acid battery make it sensitive to temperature variation. Above the operation temperature, 1^{o}C temperature rise may lead to a significant reduction on the capacity and lifespan. Based on the above analysis of temperature fields, it is observed that the maximum temperature difference between two-layer and six-layer is about 3^{o}C, which can be considered significant for the lead-acid battery. This indicates that the placement of the batteries is one of the critical factors to the thermal management of the outdoor battery cabinet.

4.4. Air vertical velocity fields

The air vertical velocity fields (illuminated by both contour and vector lines) obtained from the numerical simulation for two configurations of 24 batteries are shown in Figs. 10 and 11. From Figs.

10(a) and 11(a), the overall air vertical velocity fields on the symmetry planes of X = 0.40 m are not symmetrical between front vertical wall and back vertical cold wall. For the two-layer configuration, there is a weak air circulation from front vertical wall to back vertical cold wall and the air velocities in the narrow gaps between the batteries are quite small which indicates that the heat transfer between battery packs and surrounding air is rather weak. And, air flows downward along back vertical cold wall and upward along front vertical wall, and its velocity does not increase with the reduction of height and decrease with the growth of height because of the effect of concentration heat. As for six-layer configuration, however, there is a stronger air circulation from battery packs to the back vertical cold wall. In addition, the air velocities increase along the battery packs and reach a maximum value at the top of the battery cabinet due to the effect of concentration heat which implies that the heat transfer between battery packs and surrounding air is rather stronger. As ambient temperature set at 50^{o}C, Fig. 10(b) shows the overall air vertical velocity field is similar to the first case (T_{amb} = 30^{o}C) but the maximum velocities of upward airflow and downward airflow are higher than those of the first case (0.18 m/s VS 0.12 m/s; -0.08 m/s VS -0.05 m/s). The reason is that higher ambient temperature increases the temperature difference between the hot air near front vertical wall and the cold air near back vertical cold wall, which enhances natural convection from front vertical wall to back vertical cold wall in battery cabinet.

As shown in Figs. 10(c) and 11(c), the air vertical velocity fields on the symmetry planes of Y = 0.42 m are symmetrical between left vertical cold wall and right vertical cold wall. For the two-layer configuration, there are four local small air circulations enhancing the heat transfer between battery packs and surrounding air. This observation is in agreement with the temperature field shown in Fig. 8(a) that air temperatures are homogeneous among the top, bottom of the battery cabinet and the gap of two layers. The maximum velocities of upward airflow and downward airflow are 0.08 m/s and -0.04 m/s respectively. As for six-layer configuration, however, the cold air downwards along the cold wall and the warm air upwards from the gaps between two vertical batteries packs, which causes thermal stratification in the cold zone at the bottom of the battery cabinet and the warm zone at the top. This is according with the air temperature field shown in Fig. 9(a). The maximum velocities of upward airflow and downward airflow are 0.16 m/s and -0.04 m/s respectively. As ambient temperature set at 50^{o}C, it can be seen from Figs. 10(d) and 11(d) that the air vertical velocity fields are similar to the

first case (T_{amb} = 30°C).

5. Conclusions

The flow field and temperature distribution inside the battery cabinet are investigated by the experiments and the numerical simulations for two-layer and six-layer configurations containing 24 batteries. The experiment focuses on the surface temperature of battery packs, while the measured cold wall temperatures are used as the boundary conditions in the numerical study. For this study, the surface temperatures of battery packs based on the numerical model are slightly higher than those obtained by experiment with a deviation less than 5%.

The comparison of the experimental data with the numerical simulations confirms that the CFD model can be used to predict accurately the air velocity and temperature fields on different planes in battery cabinet. The following conclusions can be drawn from this study:

(i) The passive air cooling system utilizing natural convection is capable of maintaining battery temperature at optimal values between 20°C and 30°C.

(ii) The overall temperature field under six-layer arrangement is more even than that under two-layer arrangement due to the uniform arrangement for 24 batteries from bottom wall to top wall. The maximum temperature under two-layer arrangement is higher than that under six-layer arrangement due to 12 batteries of each layer arranged tightly forming a large concentration heat.

(iii) For the configuration of two-layer, there is the main air circulation from the front vertical wall to the back vertical cold wall which will be affected significantly by the higher external temperature.

(iv) The air circulation from the front vertical wall to the back vertical cold wall is weaken due to intensive six-layer arrangement for 24 batteries. In addition, high temperature does not significantly influence the overall air vertical velocity fields, which is different from the configuration of two-layer.

(v) Uniform arrangement of 24 batteries with larger distance between batteries, batteries and front vertical wall, batteries and top wall along the height direction could easily strengthen the interior air circulations due to the enhanced buoyancy effect. These findings can be applied to maintain outdoor battery cabinet within the proper working temperature by natural convective heat transfer.

Acknowledgement

This work was supported by Science and Technology Project of Shaanxi Province (2014JZ-002)

and Foundation of Key Laboratory of Renewable Energy Utilization Technologies in Buildings of the National Education Ministry in Shandong Jianzhu University.

References

[1] M. Maja, G. Morello, P. Spinelli, A model for simulating fast charging of lead/acid batteries, Journal of Power Sources, 40(1–2) (1992) 81-91.
[2] A.A. Pesaran, A. Vlahinos, S.D. Burch, Thermal performance of EV and HEV battery modules and packs, National Renewable Energy Laboratory, 1997.
[3] R.K. Jaworski, J.M. Hawkins, Thermal runaway behaviour of VRLA batteries, in: Telecommunications Energy Conference, 1996. INTELEC'96., 18th International, IEEE, 1996, pp. 45-51.
[4] C. Alaoui, Z.M. Salameh, A novel thermal management for electric and hybrid vehicles, Vehicular Technology, IEEE Transactions on, 54(2) (2005) 468-476.
[5] A.S. Keller, G. Whitehead, Thermal characteristics of electric vehicle batteries, SAE Technical Paper, 1991.
[6] D. Linden, Handbook of batteries and fuel cells, New York, McGraw-Hill Book Co., 1984, 1075 p. No individual items are abstracted in this volume., 1 (1984).
[7] R. Mahamud, C. Park, Reciprocating air flow for Li-ion battery thermal management to improve temperature uniformity, Journal of Power Sources, 196(13) (2011) 5685-5696.
[8] A.A. Pesaran, Battery thermal management in EV and HEVs: issues and solutions, Battery Man, 43(5) (2001) 34-49.
[9] A.A. Pesaran, S. Burch, M. Keyser, An approach for designing thermal management systems for electric and hybrid vehicle battery packs, Proceedings of the 4th Vehicle Thermal Management Systems, (1999) 24-27.
[10] R. Sabbah, R. Kizilel, J. Selman, S. Al-Hallaj, Active (air-cooled) vs. passive (phase change material) thermal management of high power lithium-ion packs: Limitation of temperature rise and uniformity of temperature distribution, Journal of Power Sources, 182(2) (2008) 630-638.
[11] S. Al-Hallaj, J. Selman, Thermal modeling of secondary lithium batteries for electric vehicle/hybrid electric vehicle applications, Journal of power sources, 110(2) (2002) 341-348.
[12] A. Mills, S. Al-Hallaj, Simulation of passive thermal management system for lithium-ion battery packs, Journal of Power Sources, 141(2) (2005) 307-315.
[13] S.A. Khateeb, S. Amiruddin, M. Farid, J.R. Selman, S. Al-Hallaj, Thermal management of Li-ion battery with phase change material for electric scooters: experimental validation, Journal of Power Sources, 142(1) (2005) 345-353.
[14] G. Colomer, M. Costa, R. Consul, A. Oliva, Three-dimensional numerical simulation of convection and radiation in a differentially heated cavity using the discrete ordinates method, International Journal of heat and Mass Transfer, 47 (2004) 257-269.
[15] O. Laguerre, S. Ben Amara, J. Moureh, D. Flick, Numerical simulation of air flow and heat transfer in domestic refrigerators, Journal of Food Engineering, 81 (2007) 144-156.

Tables

Table 1 Boundary conditions for numerical simulations

Surface	**Ambient Temperature**	
	30ºC	50ºC
Front vertical wall	4.97 W/m^2	21.3 W/m^2
Back vertical cold wall	17ºC	17ºC
Left vertical cold wall	17ºC	17ºC
Right vertical cold wall	17 ºC	17ºC
Top horizontal wall	4.97 W/m^2	21.3 W/m^2
Bottom horizontal wall	4.97 W/m^2	21.3 W/m^2
Battery packs	8.72 W/m^2	8.72 W/m^2

Table 2 Computational meshes

Mesh number	Height (173cm)	Length (80cm)	Width (84cm)	Total
Two-layer	180	82	168	2479680
Six-layer	180	164	90	2656800

Figure captions

Fig. 1 Schematic diagrams, (a) the battery cabinet, temperature-controlled chamber and refrigeration system and (b) internal dimensions (in mm) of the battery cabinet.

Fig. 2 The schematic diagrams of the two batteries arrangements: (a) two-layer and (b) six-layer.

Fig. 3 Locations of thermocouples: (a) Z = 1.1 m plane of two-layer configuration, (b) Z = 0.33 m plane of two-layer configuration, (c) Y = 0.42 m plane of six-layer configuration.

Fig. 4 Locations of thermocouples on the internal surfaces of the cold walls (a) on the symmetry plane of the side walls at Y = 0.42 m of the battery cabinet and (b) on the symmetry plane of the back wall at X = 0.40 m of the battery cabinet.

Fig. 5 The horizontal temperature profiles over two heights with cold walls temperature maintained at 17^{o}C for (a) T_{amb} = 30^{o}C and (b) T_{amb} = 50^{o}C

Fig. 6 The vertical temperature profiles over two positions on the center plane of Y = 0.42 m of battery cabinet with cold walls temperatures maintained at 17^{o}C for (a) T_{amb} = 30^{o}C and (b) T_{amb} = 50^{o}C

Fig. 7 Comparisons between measured and simulated surface temperatures of battery packs with ambient temperature maintained at 30^{o}C for (a) Z = 0.33 m with two-layer configuration, (b) X = 0.215 m with six-layer configuration

Fig. 8 Predicted temperature fields with the configuration of two-layer for 24 batteries: (a) on the symmetry plane at Y = 0.42 m of battery cabinet with T_{amb} = 30^{o}C, (b) on the symmetry plane at Y = 0.42 m of battery cabinet with T_{amb} = 50^{o}C, (c) on the symmetry plane at X = 0.40 m of battery cabinet with T_{amb} = 30^{o}C, (d) on the symmetry plane at X = 0.40 m of battery cabinet with T_{amb}= 50^{o}C.

Fig. 9 Predicted temperature fields with the configuration of six-layer for 24 batteries: (a) on the symmetry plane at Y = 0.42 m of battery cabinet with T_{amb} = 30^{o}C, (b) on the symmetry plane at Y = 0.42 m of battery cabinet with T_{amb} = 50^{o}C, (c) on the symmetry plane at X = 0.40 m of battery cabinet with T_{amb} = 30^{o}C, (d) on the symmetry plane at X = 0.40 m of battery cabinet with T_{amb} = 50^{o}C.

Fig. 10 Predicted vertical velocity fields with the configuration of two-layer for 24 batteries: (a) on the symmetry plane at X = 0.40 m of battery cabinet with T_{amb} = 30^{o}C, (b) on the symmetry plane at X = 0.40 m of battery cabinet with T_{amb} = 50^{o}C, (c) on the symmetry plane at Y = 0.42 m of battery cabinet with T_{amb} = 30^{o}C, (d) on the symmetry plane at Y = 0.42 m of battery cabinet with T_{amb} = 50^{o}C.

Fig. 11 Predicted vertical velocity fields with the configuration of six-layer for 24 batteries: (a) on the symmetry plane at X = 0.40 m of battery cabinet with T_{amb} = 30^{o}C, (b) on the symmetry plane at X = 0.40 m of battery cabinet with T_{amb} = 50^{o}C, (c) on the symmetry plane at Y = 0.42 m of battery cabinet with T_{amb} = 30^{o}C, (d) on the symmetry plane at Y = 0.42 m of battery cabinet with T_{amb} = 50^{o}C.

Figures

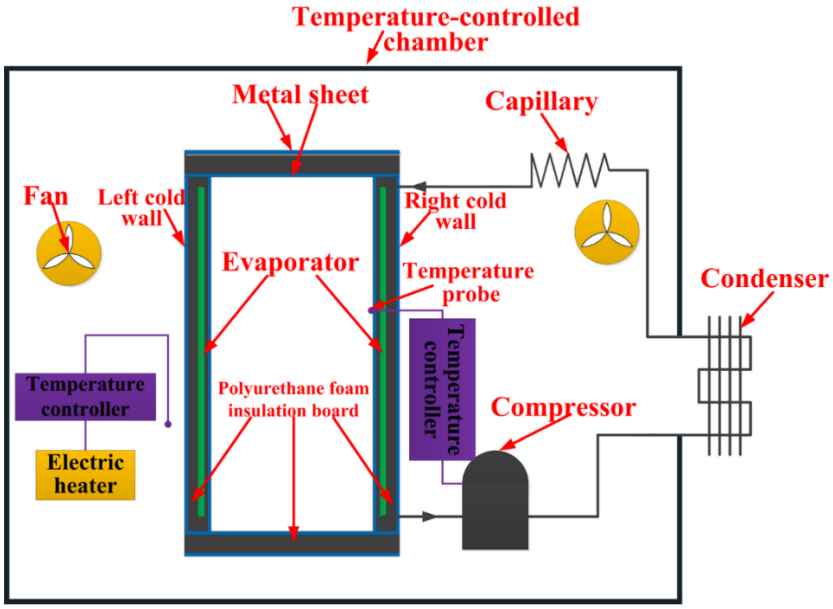

(a)

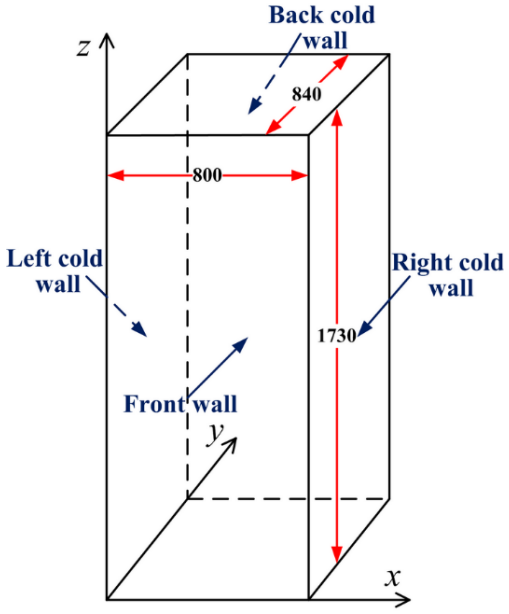

(b)

Fig. 1 Schematic diagrams, (a) the battery cabinet, temperature-controlled chamber and refrigeration system and (b) internal dimensions (in mm) of the battery cabinet.

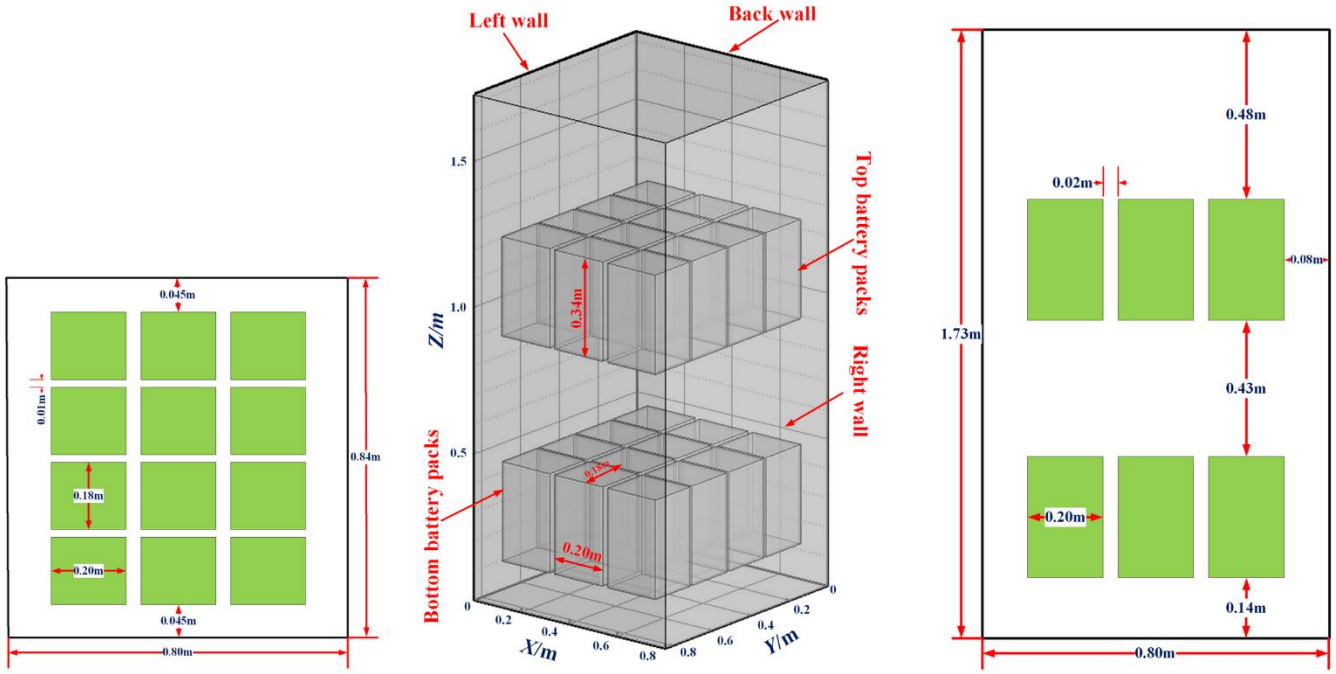

(a)

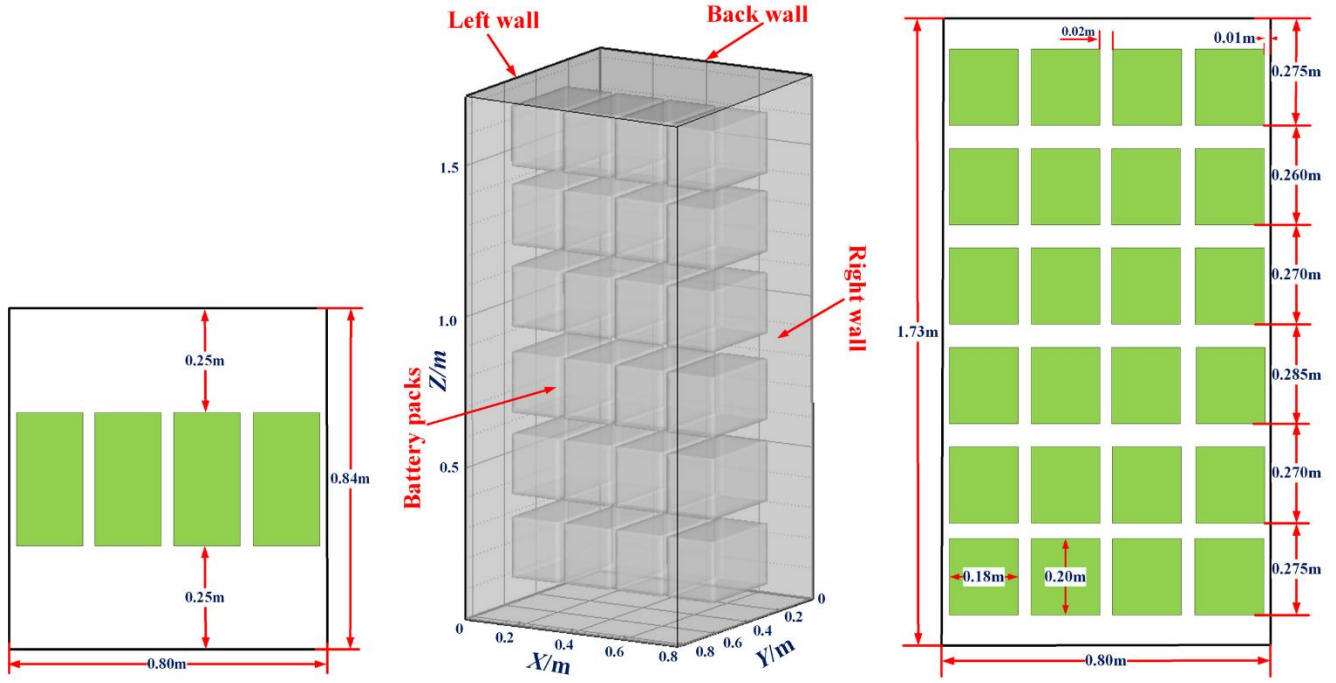

(b)

Fig. 2 The schematic diagrams of the two batteries arrangements: (a) two-layer and (b) six-layer.

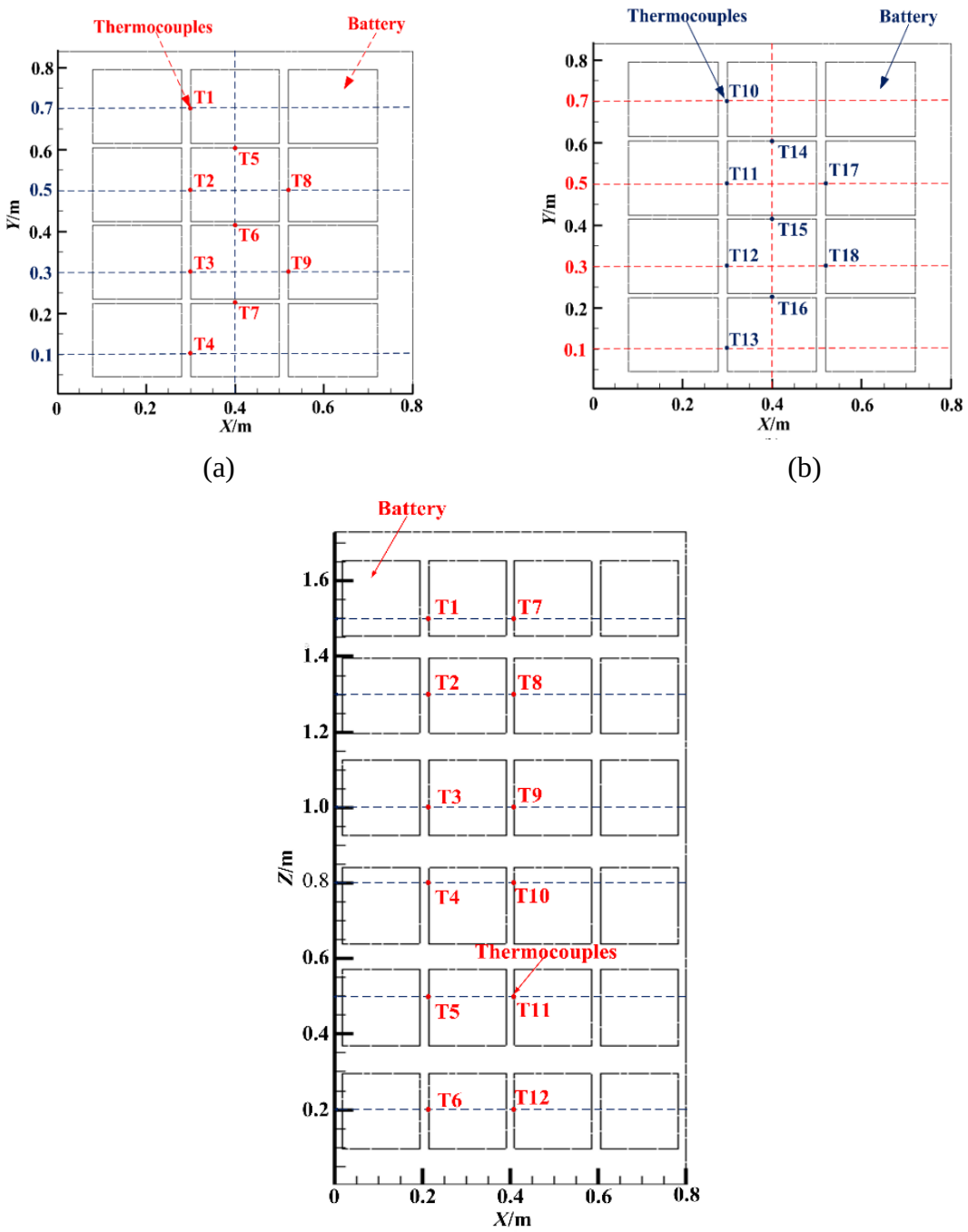

Fig. 3 Locations of thermocouples: (a) Z = 1.1 m plane of two-layer configuration, (b) Z = 0.33 m plane of two-layer configuration, (c) Y = 0.42 m plane of six-layer configuration.

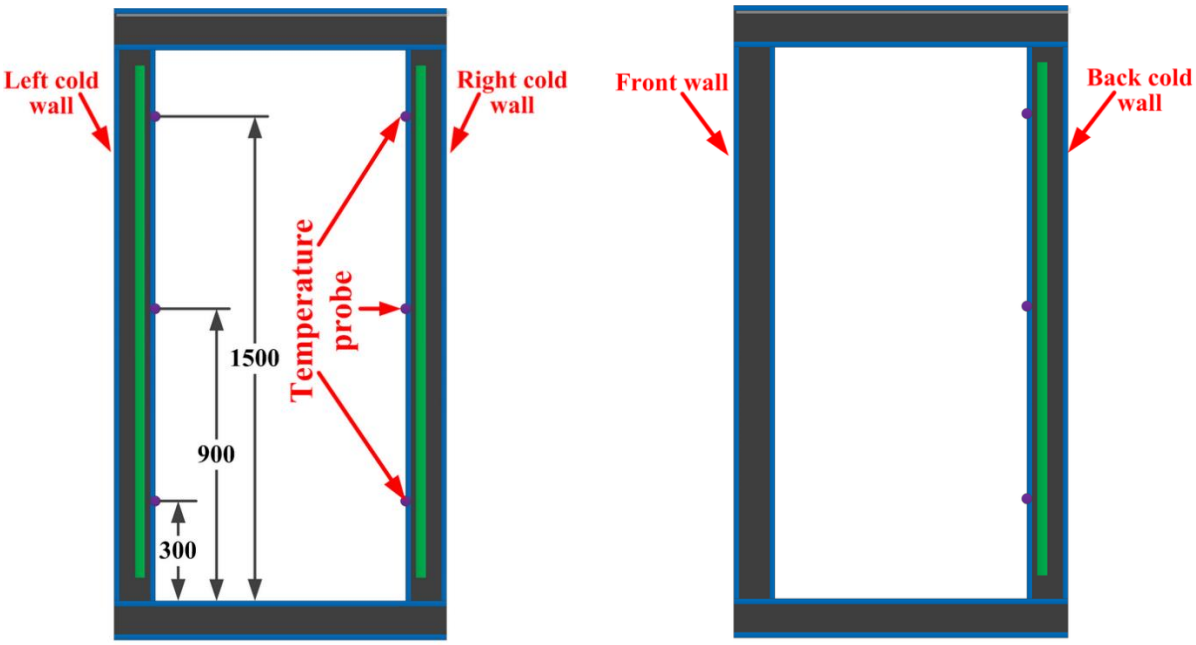

Fig. 4 Locations of thermocouples on the internal surfaces of the cold walls (a) on the symmetry plane of the side walls at Y = 0.42 m of the battery cabinet and (b) on the symmetry plane of the back wall at X = 0.40 m of the battery cabinet.

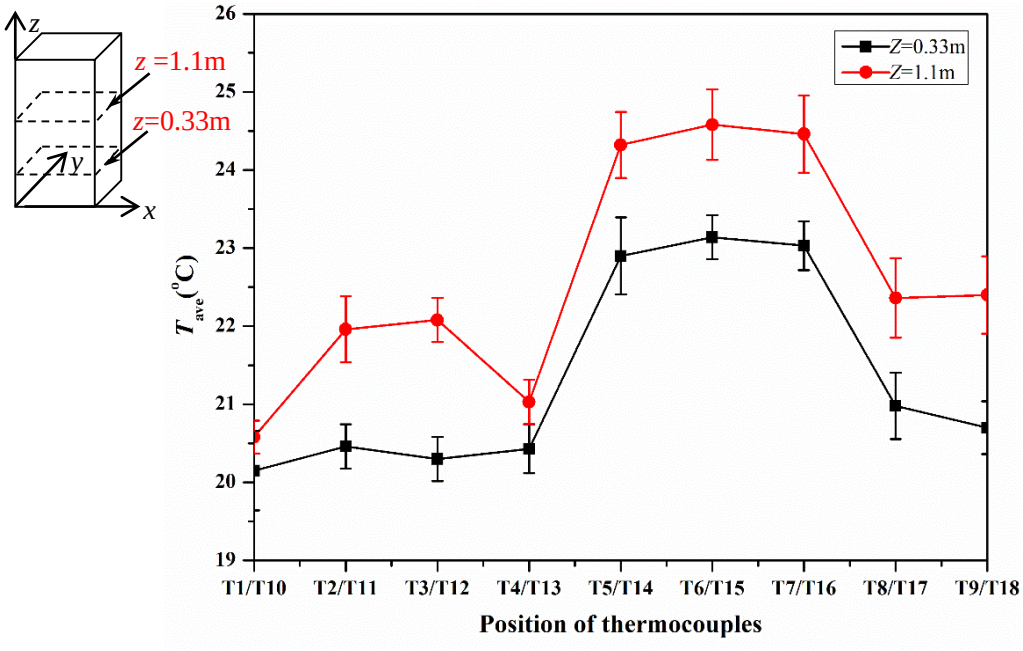

(a)

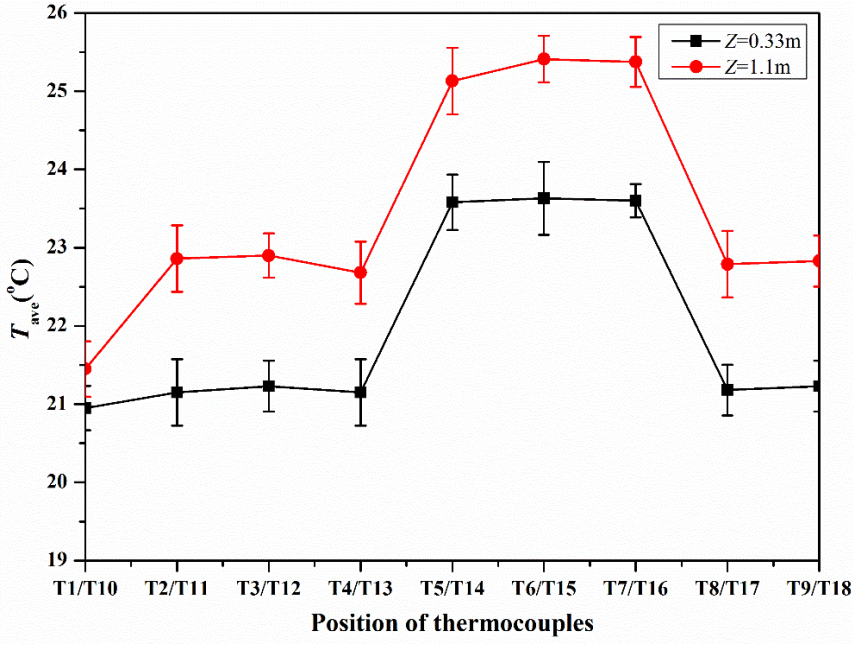

(b)

Fig. 5 The horizontal temperature profiles over two heights with cold walls temperature maintained at 17°C for (a) T_{amb} = 30°C and (b) T_{amb} = 50°C

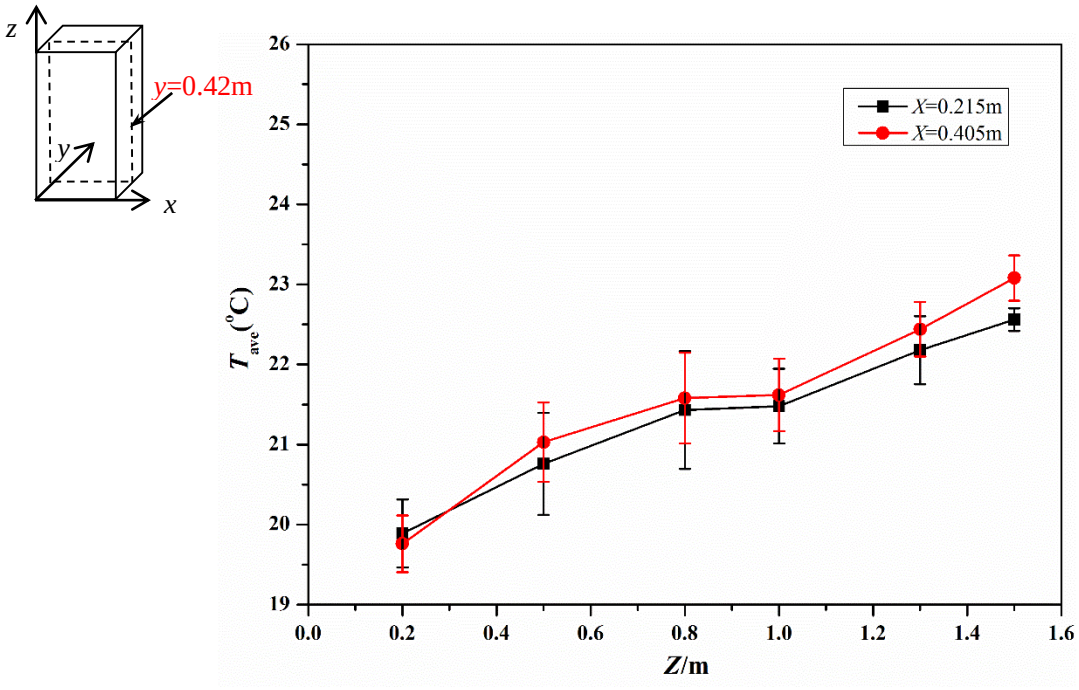

(a)

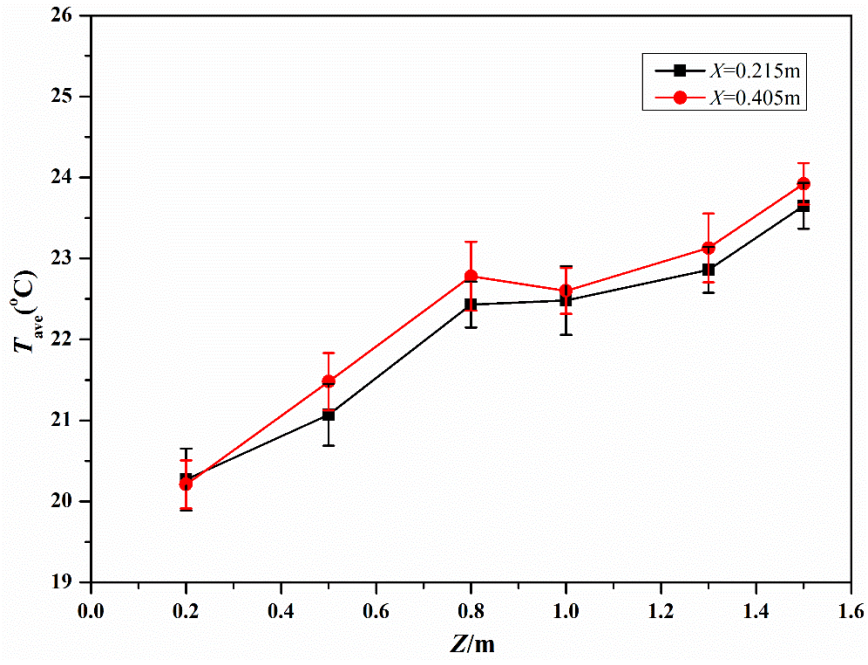

(b)

Fig. 6 The vertical temperature profiles over two positions on the center plane of Y = 0.42 m of battery cabinet with cold walls temperatures maintained at 17°C for (a) T_{amb} = 30°C and (b) T_{amb} = 50°C

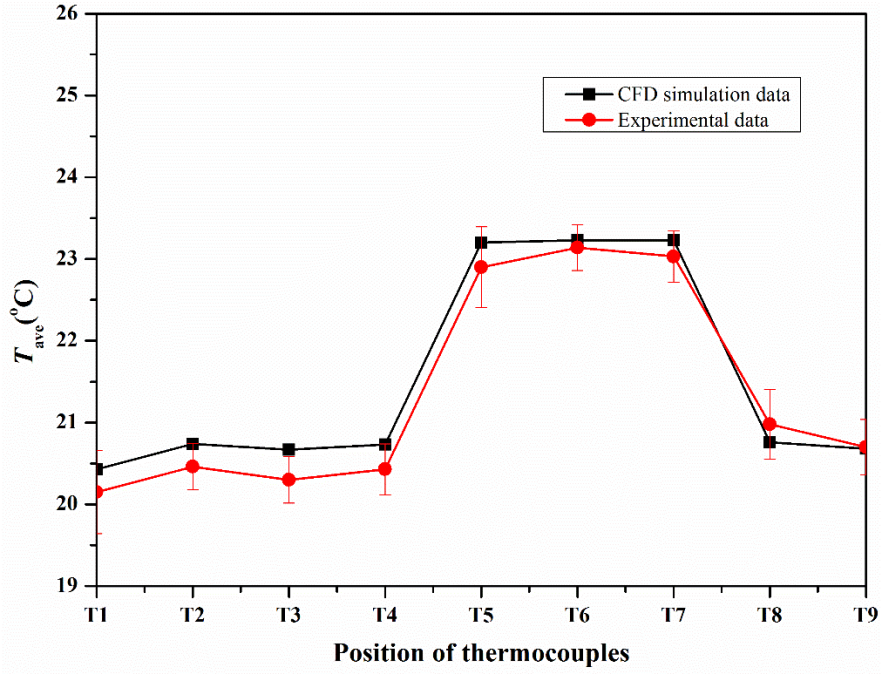

(a)

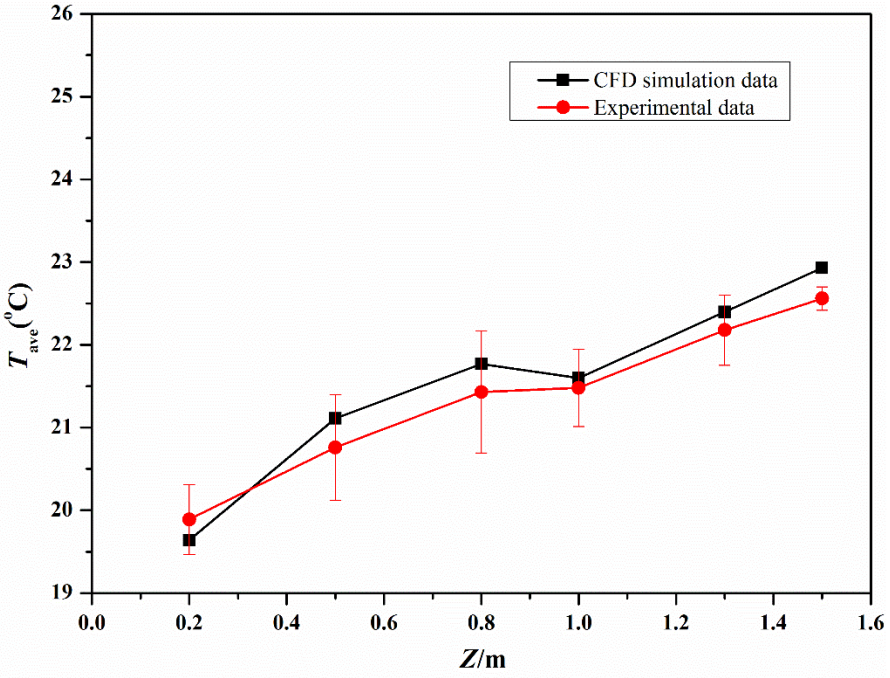

(b)

Fig. 7 Comparisons between measured and simulated surface temperatures of battery packs with ambient temperature maintained at 30°C for (a) Z = 0.33 m with two-layer configuration, (b) X = 0.215 m with six-layer configuration

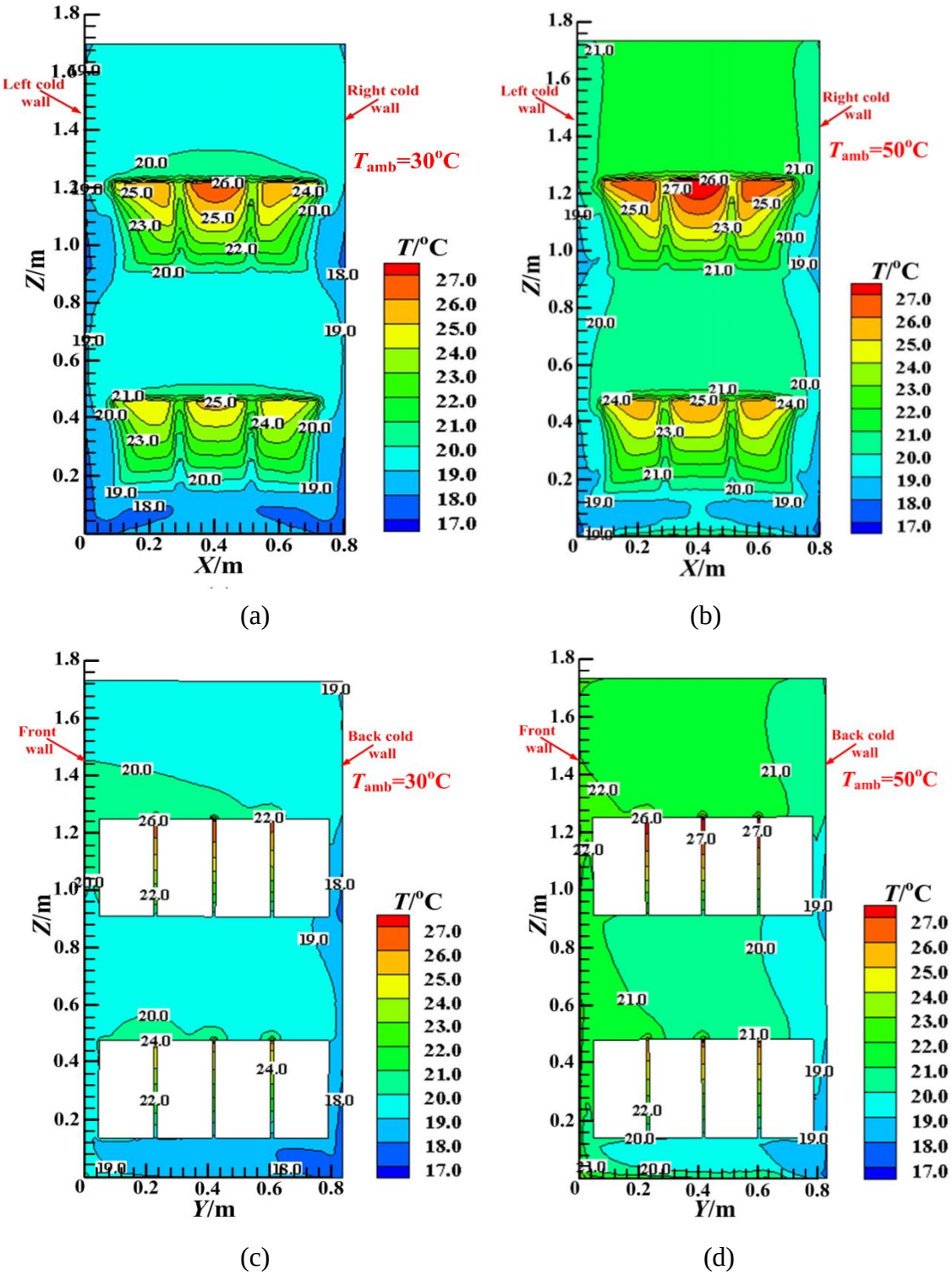

Fig. 8 Predicted temperature fields with the configuration of two-layer for 24 batteries: (a) on the symmetry plane at Y = 0.42 m of battery cabinet with T_{amb} = 30°C, (b) on the symmetry plane at Y = 0.42 m of battery cabinet with T_{amb} = 50°C, (c) on the symmetry plane at X = 0.40 m of battery cabinet with T_{amb} = 30°C, (d) on the symmetry plane at X = 0.40 m of battery cabinet with T_{amb}= 50°C.

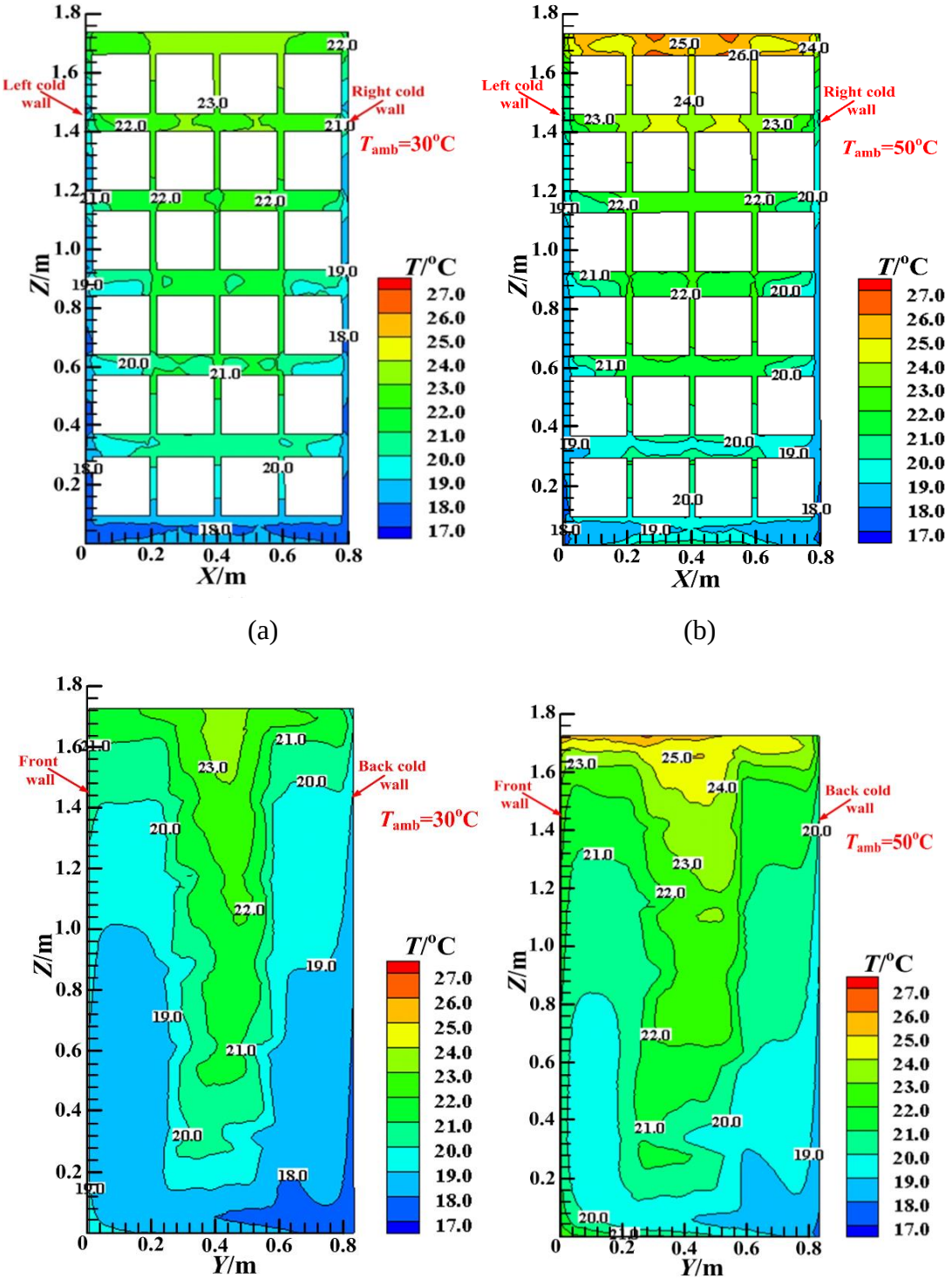

Fig. 9 Predicted temperature fields with the configuration of six-layer for 24 batteries: (a) on the symmetry plane at Y = 0.42 m of battery cabinet with T_{amb} = 30°C, (b) on the symmetry plane at Y = 0.42 m of battery cabinet with T_{amb} = 50°C, (c) on the symmetry plane at X = 0.40 m of battery cabinet with T_{amb} = 30°C, (d) on the symmetry plane at X = 0.40 m of battery cabinet with T_{amb} = 50°C.

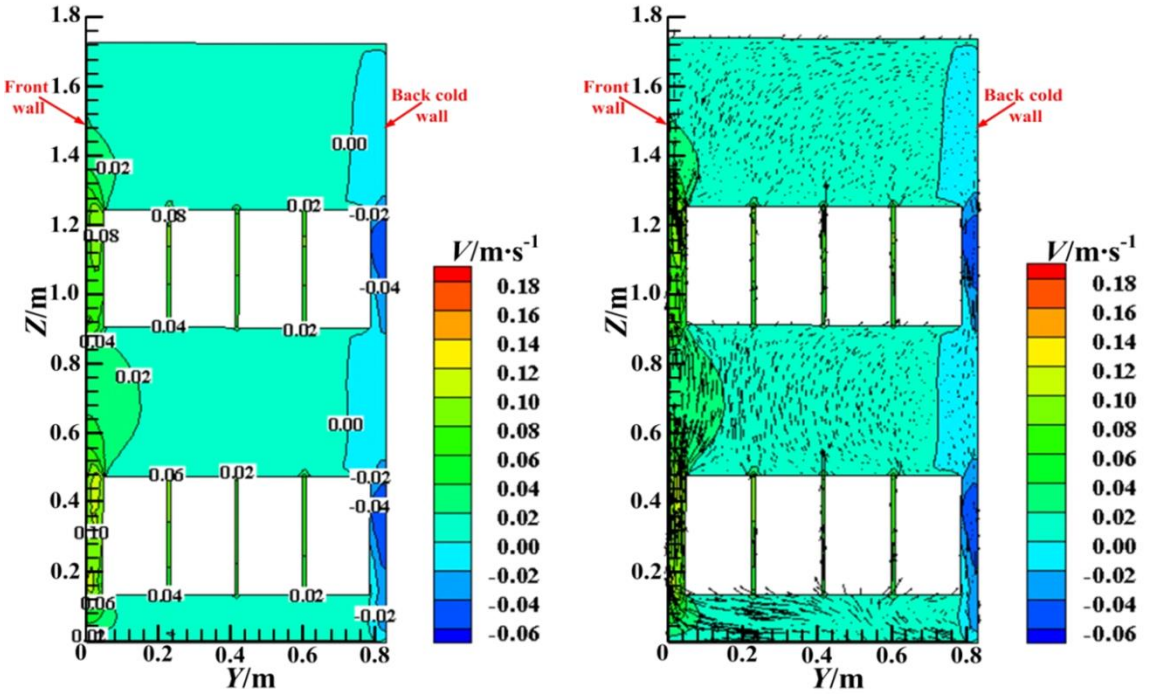
Front wall
Back cold wall
Z/m
Y/m
V/m·s-1
0.18
0.16
0.14
0.12
0.10
0.08
0.06
0.04
0.02
0.00
-0.02
-0.04
-0.06

(a)

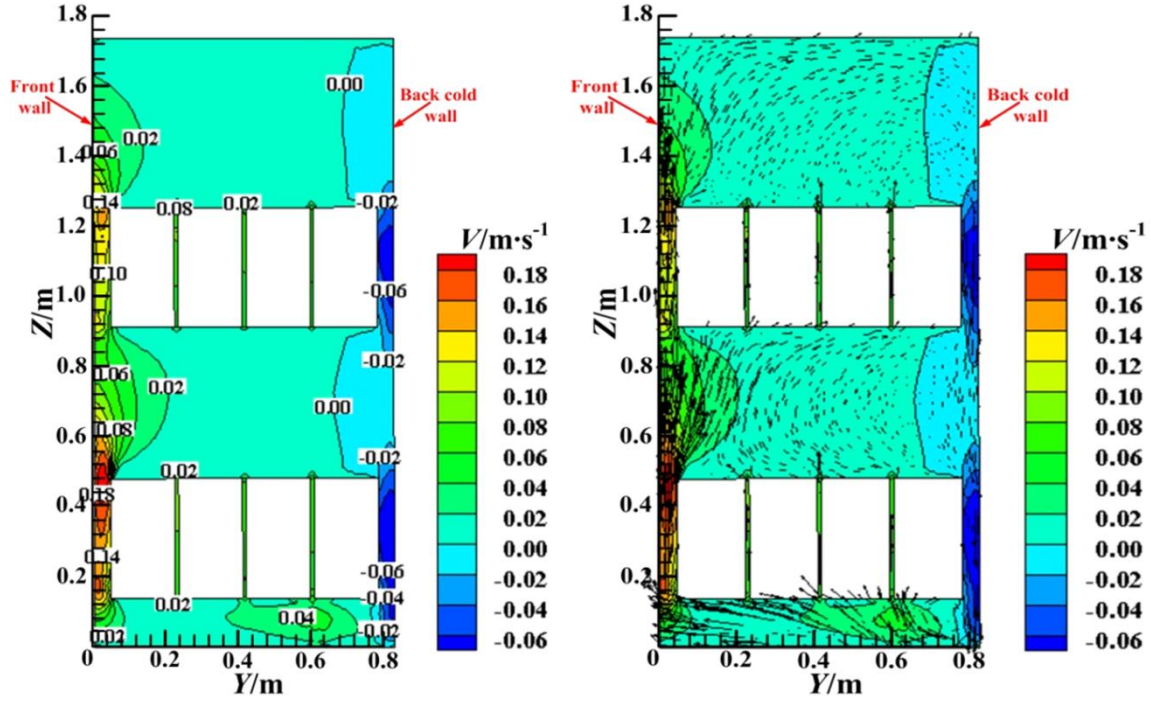
Front wall
Back cold wall
Z/m
Y/m
V/m·s-1
0.18
0.16
0.14
0.12
0.10
0.08
0.06
0.04
0.02
0.00
-0.02
-0.04
-0.06

(b)

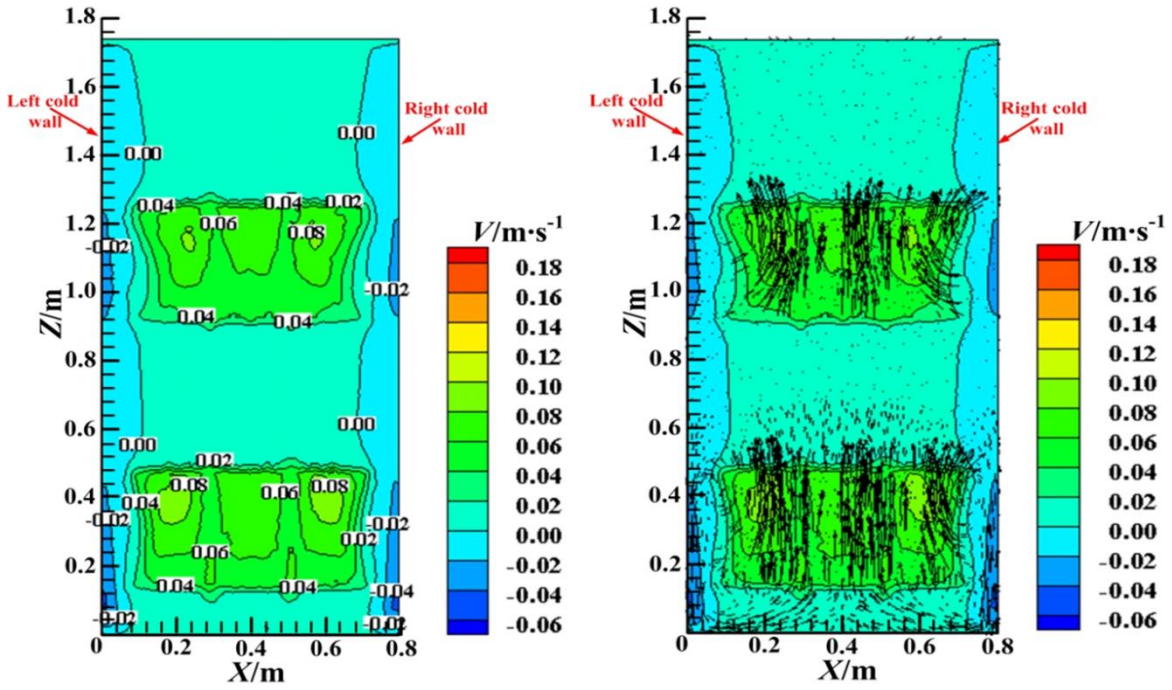

(c)

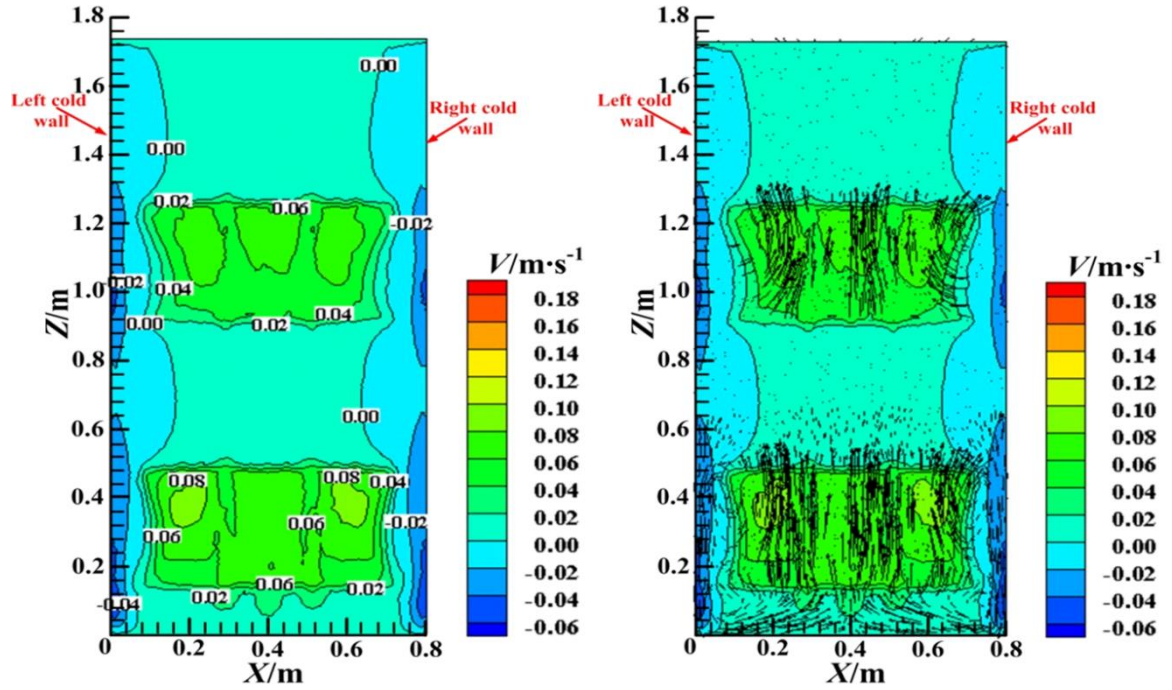

(d)

Fig. 10 Predicted vertical velocity fields with the configuration of two-layer for 24 batteries: (a) on the symmetry plane at X = 0.40 m of battery cabinet with T_{amb} = 30°C, (b) on the symmetry plane at X = 0.40 m of battery cabinet with T_{amb} = 50°C, (c) on the symmetry plane at Y = 0.42 m of battery cabinet with T_{amb} = 30°C, (d) on the symmetry plane at Y = 0.42 m of battery cabinet with T_{amb} = 50°C.

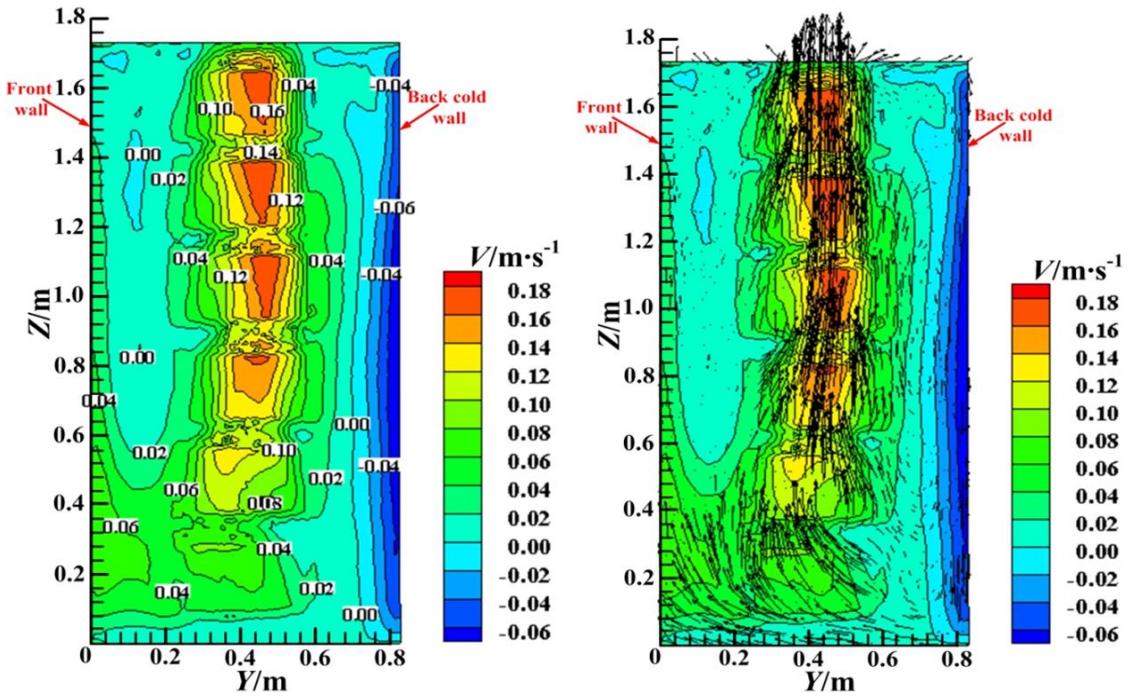
Front wall
Back cold wall
Z/m
Y/m
V/m·s-1
0.18
0.16
0.14
0.12
0.10
0.08
0.06
0.04
0.02
0.00
-0.02
-0.04
-0.06

(a)

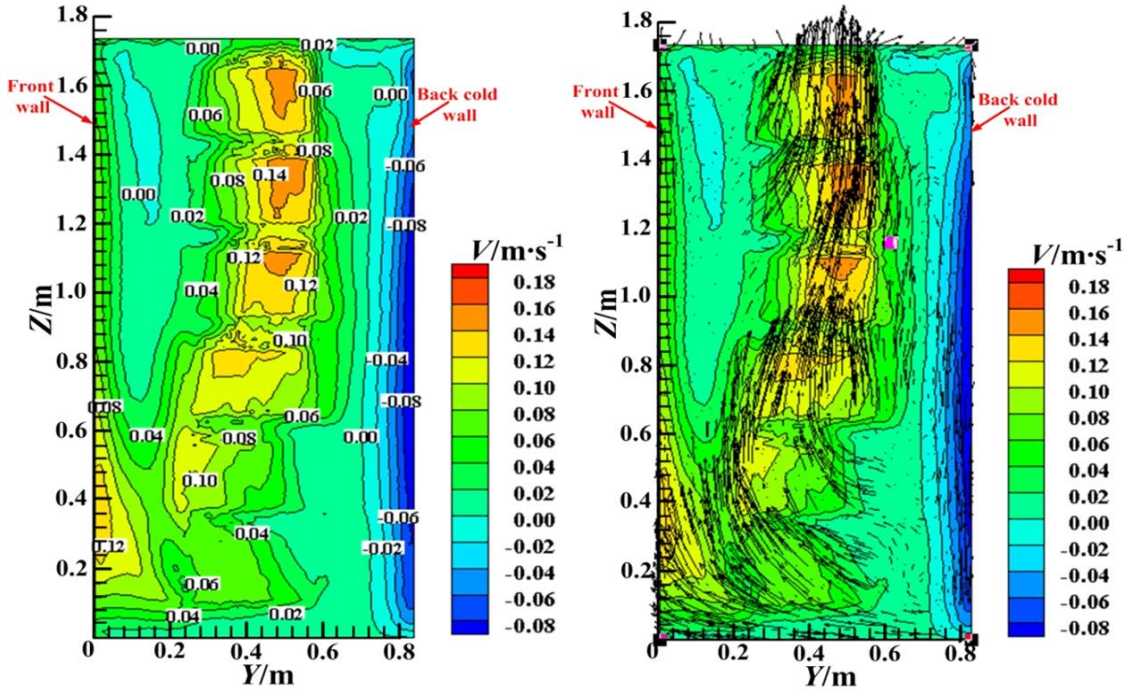
Front wall
Back cold wall
Z/m
Y/m
V/m·s-1
0.18
0.16
0.14
0.12
0.10
0.08
0.06
0.04
0.02
0.00
-0.02
-0.04
-0.06
-0.08

(b)

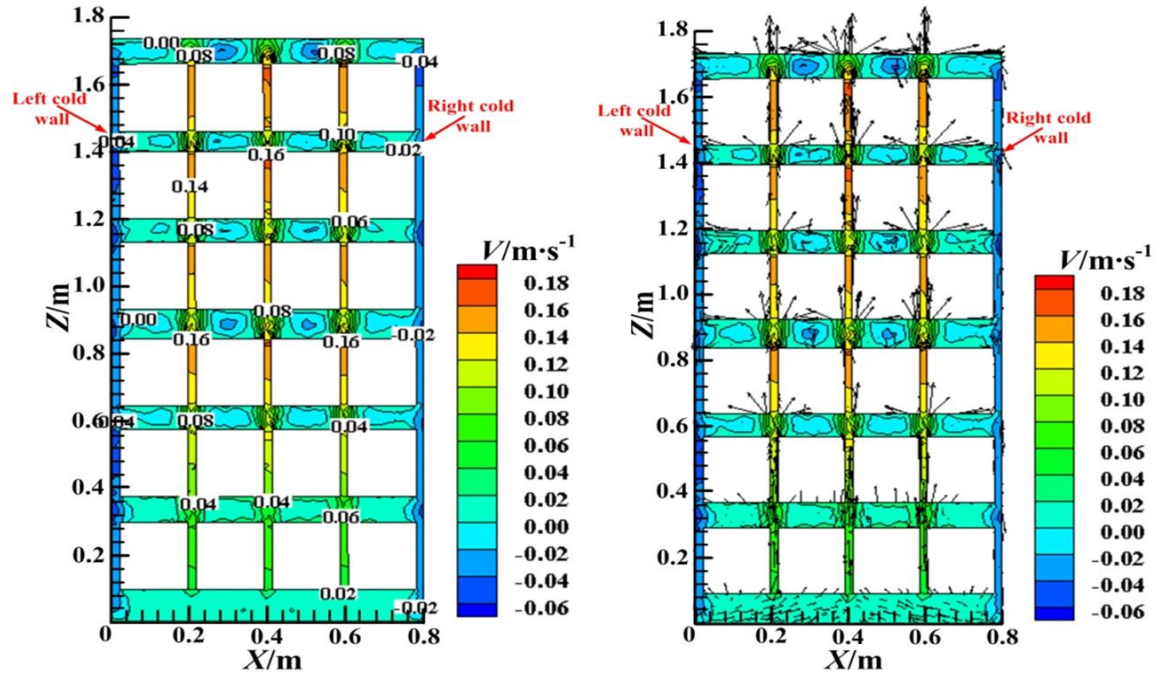

(c)

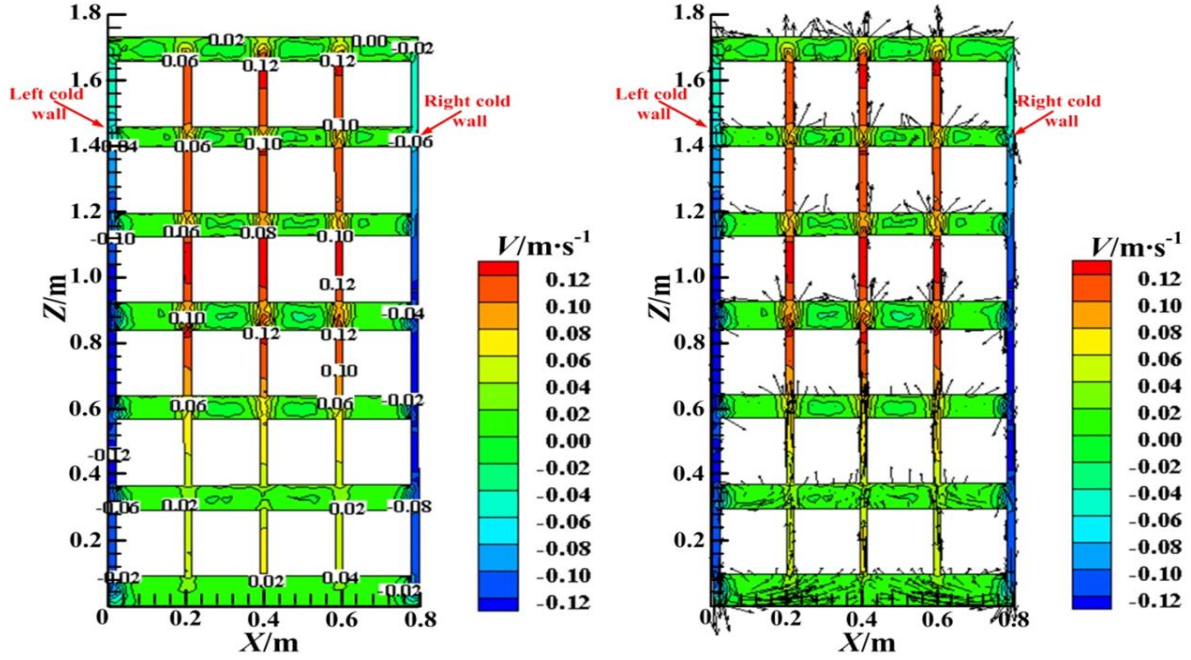

(d)

Fig. 11 Predicted vertical velocity fields with the configuration of six-layer for 24 batteries: (a) on the symmetry plane at X = 0.40 m of battery cabinet with T_{amb} = 30°C, (b) on the symmetry plane at X = 0.40 m of battery cabinet with T_{amb} = 50°C, (c) on the symmetry plane at Y = 0.42 m of battery cabinet with T_{amb} = 30°C, (d) on the symmetry plane at Y = 0.42 m of battery cabinet with T_{amb} = 50°C.